Expedite your small-field dosimetry workflow.

SRS MapCHECK™

SRS PATIENT QA, NO FILM

See it firsthand at AAPM 2018

Learn More

SUN NUCLEAR corporation

Distortion-free diffusion MRI using an MRI-guided Tri-Cobalt 60 radiotherapy system: Sequence verification and preliminary clinical experience

Yu Gao
Department of Radiological Sciences, University of California, Los Angeles, CA, USA
Physics and Biology in Medicine IDP, University of California, Los Angeles, CA, USA

Fei Han and Ziwu Zhou
Department of Radiological Sciences, University of California, Los Angeles, CA, USA

Minsong Cao
Department of Radiation Oncology, University of California, Los Angeles, CA, USA
Physics and Biology in Medicine IDP, University of California, Los Angeles, CA, USA

Tania Kaprealian, Mitchell Kamrava, Chenyang Wang, and John Neylon
Department of Radiation Oncology, University of California, Los Angeles, CA, USA

Daniel A. Low and Yingli Yang
Department of Radiation Oncology, University of California, Los Angeles, CA, USA
Physics and Biology in Medicine IDP, University of California, Los Angeles, CA, USA

Peng Hu[a)]
Department of Radiological Sciences, University of California, Los Angeles, CA, USA
Physics and Biology in Medicine IDP, University of California, Los Angeles, CA, USA

(Received 8 May 2017; revised 19 June 2017; accepted for publication 4 July 2017; published 12 August 2017)

Purpose: Monitoring tumor response during the course of treatment and adaptively modifying treatment plan based on tumor biological feedback may represent a new paradigm for radiotherapy. Diffusion MRI has shown great promises in assessing and predicting tumor response to radiotherapy. However, the conventional diffusion-weighted single-shot echo-planar-imaging (DW-ssEPI) technique suffers from limited resolution, severe distortion, and possibly inaccurate ADC at low field strength. The purpose of this work was to develop a reliable, accurate and distortion-free diffusion MRI technique that is practicable for longitudinal tumor response evaluation and adaptive radiotherapy on a 0.35 T MRI-guided radiotherapy system.

Methods: A diffusion-prepared turbo spin echo readout (DP-TSE) sequence was developed and compared with the conventional diffusion-weighted single-shot echo-planar-imaging sequence on a 0.35 T MRI-guided radiotherapy system (ViewRay). A spatial integrity phantom was used to quantitate and compare the geometric accuracy of the two diffusion sequences for three orthogonal orientations. The apparent diffusion coefficient (ADC) accuracy was evaluated on a diffusion phantom under both 0 °C and room temperature to cover a diffusivity range between 0.40×10^{-3} and 2.10×10^{-3} mm^2/s. Ten room temperature measurements repeated on five different days were conducted to assess the ADC reproducibility of DP-TSE. Two glioblastoma (GBM) and six sarcoma patients were included to examine the in vivo feasibility. The target registration error (TRE) was calculated to quantitate the geometric accuracy where structural CT or MR images were co-registered to the diffusion images as references. ADC maps from DP-TSE and DW-ssEPI were calculated and compared. A tube phantom was placed next to patients not treated on ViewRay, and ADCs of this reference tube were also compared.

Results: The proposed DP-TSE passed the spatial integrity test (< 1 mm within 100 mm radius and < 2 mm within 175 mm radius) under the three orthogonal orientations. The detected errors were 0.474 ± 0.355 mm, 0.475 ± 0.287 mm, and 0.546 ± 0.336 mm in the axial, coronal, and sagittal plane. DW-ssEPI, however, failed the tests due to severe distortion and low signal intensity. Noise correction must be performed for the DW-ssEPI to avoid ADC quantitation errors, whereas it is optional for DP-TSE. At 0 °C, the two sequences provided accurate quantitation with < 3% variation with the reference. In the room temperature study, discrepancies between ADCs from DP-TSE and the reference were within 4%, but could be as high as 8% for DW-ssEPI after the noise correction. Excellent ADC reproducibility with a coefficient of variation < 5% was observed among the 10 measurements of DP-TSE, indicating desirable robustness for ADC-based tumor response assessment. In vivo TRE in DP-TSE was less than 1.6 mm overall, whereas it could be greater than 12 mm in DW-ssEPI. For GBM patients, the CSF and brain tissue ADCs from DP-TSE were within the ranges found in literature. ADC differences between the two techniques were within 8% among the six

sarcoma patients. For the reference tube that had a relatively low diffusivity, the two diffusion sequences provided matched measurements.

Conclusion: A diffusion technique with excellent geometric fidelity, accurate, and reproducible ADC measurement was demonstrated for longitudinal tumor response assessment using a low-field MRI-guided radiotherapy system. [https://doi.org/10.1002/mp.12465]

Key words: adaptive radiotherapy, distortion-free diffusion MRI, treatment response

1. INTRODUCTION

Diffusion MRI is a promising imaging technique for assessing and predicting tumor response to radiotherapy,[1,2] often well before macroscopic changes in tumor size and morphology[3,4]. The changes in the apparent diffusion coefficient (ADC) during the course of radiotherapy have been shown to correlate with tumor control and treatment outcome[5–7]. Therefore, diffusion MRI is an important imaging biomarker for tumor response for which the treatment plan can be adaptively altered during therapy. As such, functional MRI-based adaptive therapy strategy may represent a new paradigm for radiotherapy.

To enable widespread use of diffusion MRI-guided adaptive therapy, several scientific challenges need to be overcome. For example, the optimal timing for imaging needs to be established. A number of previous studies of diffusion MRI for predicting tumor response to radiotherapy focused on performing diffusion MRI at selected time points before, during and after the radiotherapy[6–11]. More recently, a longitudinal diffusion MRI approach has been proposed by Yang et al.[12]. In this approach, diffusion MRI is acquired every 2–5 days throughout the course of radiotherapy using an MRI-guided radiotherapy system and a longitudinal ADC curve is constructed based on the diffusion measurements at multiple time points. Despite its promise, the diffusion-weighted single-shot echo-planar-imaging (DW-ssEPI) sequence used by Yang et al.[12] suffers from low spatial resolution and severe geometric distortion due to its single-shot EPI readout. This is particularly problematic for radiotherapy as any geometric inaccuracy could directly translate to miscalculated radiation dose and potential radiation target error if adaptive treatment planning is based on these diffusion images. In addition, at low field strength, conventional DW-ssEPI becomes inaccurate when high b-value is used due to SNR loss associated with the lower field strength, which may be problematic for fully characterizing tumors with low diffusivity. It is therefore highly desirable to develop a distortion-free diffusion MRI technique with higher signal-to-noise-ratio (SNR) for tumor response evaluation and potentially adaptive radiotherapy.

Various techniques have been developed to increase the resolution or alleviate the distortion associated with DW-ssEPI. One approach uses reduced field of view diffusion imaging[13], which is not applicable to treatment response evaluation and plan modification since a large spatial coverage is necessary for radiotherapy purposes. A diffusion-weighted line-scan technique has been used to mitigate distortion; however, it suffers from low SNR and limited resolution[14]. Reserved gradient method uses two images with reversed gradient encoding to calculate the distortion-free image[15]. The problems of this method include limited resolution and the requirement to identify the boundary which could be challenging at low field and high b-value scenarios. Readout-segmented EPI have been proposed to partially mitigate distortion and improve resolution[16]; however, it still suffers from distortion due to the phase error along the EPI readout. Multi-shot diffusion-weighted balanced steady-state free precession (bSSFP) sequence provides 3D high-resolution diffusion imaging[17,18]; however, this approach suffers from ADC inaccuracies because the diffusion sensitivity is lost as bSSFP reaches steady state.

In this study, we developed a reliable, accurate, and distortion-free diffusion sequence based on a turbo spin echo acquisition that is practicable and specifically designed for assessment of tumor response to radiotherapy.

2. METHODS AND MATERIALS

2.A. Diffusion-prepared turbo spin echo (DP-TSE) pulse sequence design

The diffusion sequence was programmed for an MR-guided radiotherapy system (MRIdian, ViewRay, Mountain View, CA, USA) with a pulse sequence programming software (IDEA version VB19, Siemens Medical Solutions, Erlangen, Germany). As illustrated in Fig. 1(a), the diffusion sequence used in this study combines a diffusion preparation module with a segmented turbo spin echo readout module, where similar approaches have been previously explored in diagnostic imaging at higher field strength (1.5 T or higher)[17–19]. The diffusion module, which was inserted at the beginning of each k-space readout segment, uses a twice-refocused spin-echo (TRSE) with diffusion gradients to generate diffusion weighting. A second refocusing pulse was added in the diffusion preparation module and the timing for each gradient was optimized to reduce eddy current effects from the diffusion gradients[20]. Crusher gradients were placed before and after each 180° RF pulse to spoil simulated echoes from imperfect refocusing. At the end of diffusion encoding, the diffusion-encoded transverse magnetization was flipped back to the longitudinal direction by a −90° RF pulse, which is immediately followed by spoilers to eliminate the remaining transverse magnetization. This strategy only modulated the longitudinal

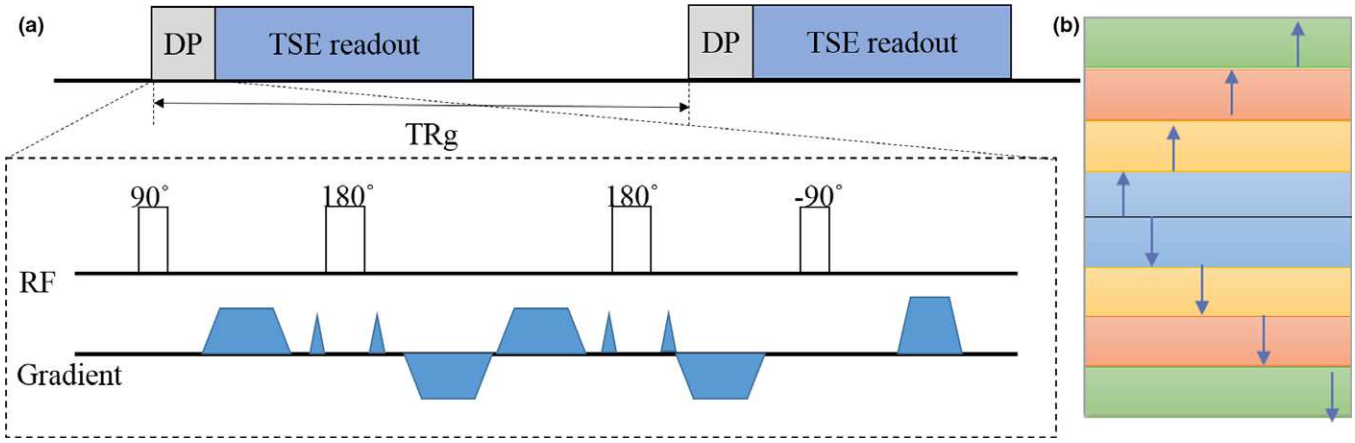

FIG. 1. Sequence diagram (a) and k-space view ordering example (b). [Color figure can be viewed at wileyonlinelibrary.com]

magnetization with diffusion weighting and no residual phase exist during the TSE readout so that the Carr-Purcell-Meiboom-Gill (CPMG) condition of TSE sequence is not violated[19]. To mitigate the signal inconsistencies between different imaging shots within the k-space, a problem frequently seen in multi-shot diffusion imaging, k-space view ordering was modified such that the central k-space is acquired by the same imaging shot[21]. Figure 1(b) is an example of a 4-shot k-space view ordering where arrows from left to right indicate the acquisition order. Lines with the same color were acquired with the same shot.

2.B. Quantitative phantom experiment

The spatial integrity, ADC accuracy and ADC reproducibility of the proposed DP-TSE technique were evaluated and compared with the standard DW-ssEPI using the 0.35 T ViewRay MR scanner with 12-channel surface coils.

2.B.1. Spatial integrity

A uniformity and linearity phantom [Fluke Biomedical, model 76-907, Fig. 2(a)] was used to assess the spatial integrity of the proposed technique under three orthogonal orientations: transverse, coronal, and sagittal. DP-TSE and DW-ssEPI images on all three orientations were acquired with field of view (FOV) = 400 × 400 mm^2. Parameters for the DW-ssEPI/DP-TSE sequences were: TR = 2000/2000 ms; TE = 160/115 ms; matrix size = 128/192; number of averages = 10/2, readout bandwidth = 752/789 Hz/pixel, echo train length (ETL) was 24 for DP-TSE (8 shots). A spatial integrity analysis tool provided by ViewRay was used to analyze the images by detecting the center location of each cylinder in the phantom based on the image and comparing the image-based location measurements with the known ground truth. Automatic rotation and translation were detected to account for setup imperfection. The geometric integrity passing criteria for each cylinder is 1 mm within 100 mm radius and 2 mm within 175 mm radius.

2.B.2. ADC accuracy

ADC accuracy of the proposed technique was compared with the conventional DW-ssEPI using a commercially available diffusion phantom (High Precision Device, Inc. Model 128). The phantom is 194 mm in radius and consists of 13 vials filled with aqueous solutions of polymer polyvinylpyrrolidone (PVP) at 0%, 10%, 20%, 30%, 40%, and 50% concentration levels [Fig. 2(b), abbreviated as vial 1 to vial 6]. The weighted mean ADC of each vial at 0 °C was provided by the manufacturer as a reference.

Both 0 °C and room temperature studies were conducted to cover a relatively wide diffusivity range. In the 0 °C study, the phantom was filled with crushed ice 1 day before the measurement and stored in a refrigerator overnight. The phantom was in the ice water bath during the imaging experiment to ensure 0 °C temperature. In the room temperature (~21.0 °C) study, the phantom was placed in the scanner room at least 2 days before the scan to allow the phantom to reach room temperature. The temperature of the phantom was measured before and after each study using an extra-long-stem thermometer through the top fill port. Only the first nine vials and the first eleven vials were analyzed in the 0 °C and room temperature studies, respectively. Vials with diffusivity lower than 0.35 × 10^{-3} mm^2/s, a number that is below the range of physiologically possible tumor ADC values, were not included.

In each study, the DW-ssEPI data were acquired at a medium resolution (MeR) of 2.34 × 2.34 × 5 mm^3 (FOV = 300 × 300 mm^2, matrix size = 128) using TR/TE = 2000/160 ms, bandwidth = 752 Hz/pixel and 17 averages. The DP-TSE data were acquired at both the same medium resolution and a higher resolution (HiR) of 1.56 × 1.56 × 5 mm^3 (FOV = 300 × 300 mm^2, matrix size = 192). The DP-TSE sequence parameters included: TR/TE = 2000/115 ms, two averages, bandwidth = 789 Hz/pixel, echo train length (ETL) = 16 for the medium resolution and 24 for the high-resolution. For both DW-ssEPI and DP-TSE, four b-values (0, 200, 500, 800 s/mm^2) were applied along the readout direction and a single TE was used

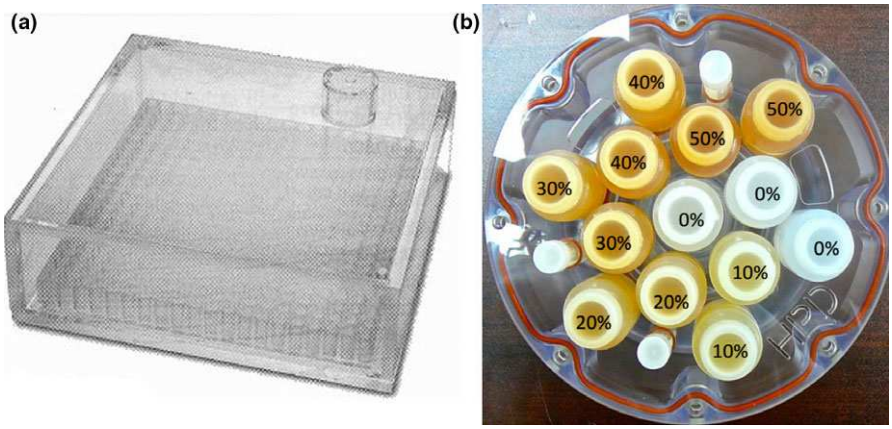

FIG. 2. Spatial integrity phantom (a) and diffusion phantom (b). The spatial integrity phantom is of dimension 33.02 × 33.02 × 10.16 cm^3 and consists of 197 cylindrical grids (20 × 20 with three missing for positioning and detecting). The diffusion phantom is 194 mm in diameter and has 13 vials with six different diffusivities. Vials with diffusivity less than 0.35 × 10^{-3} mm^2/s were not included in this study. [Color figure can be viewed at wileyonlinelibrary.com]

for all b-values within the same sequence to remove the influence of T2 on diffusion quantitation. The total scan time was 140 s for DW-ssEPI and 144s for DP-TSE. For both sequences, averaging was performed in magnitude only in the image space as complex averaging of diffusion data in k-space has been shown to cause signal loss and artifacts[22]. To obtain the reference ADC values at room temperature, the phantom was scanned with a 3 T scanner (Prisma, Siemens Medical Solution, Erlangen, Germany) using the standard DW-ssEPI sequence with FOV = 300×300 mm^2, matrix size = 160, TR/TE = 4200/76 ms, bandwidth = 1564 Hz/pixel, b = 0, 200, 500, 800, and 8 averages.

The noise subtraction method proposed by Dietrich et al.[23] was performed before ADC fitting to remove the influence of noise floor in ADC quantitation at low SNR scenario:

$$S_{nc} = \sqrt{|S_n^2 - \frac{2}{\pi}N^2|}, \quad (1)$$

where S_n and S_{nc} are noisy and noise-corrected images, N represent the average background noise signal intensity. ADC map was then calculated using the least-squares fitting of the mono-exponential curve:

$$S_{nc}(b) = S_0 e^{-b\times ADC}, \quad (2)$$

where S_{nc}(b) is noise-corrected signal intensity, b is the b-value controlled by the gradient waveform, S_0 and ADC are parameters to be fitted which correspond to signal intensity without diffusion and apparent diffusion coefficient value, respectively.

2.B.3. ADC reproducibility

To verify the reproducibility of the proposed sequence, which is essential for the robustness of the ADC-based tumor response assessment, ten room temperature studies using the high-resolution DP-TSE protocol were carried out on five different days over 3 weeks with the same phantom setup. Temperatures of the phantom were recorded before and after each scan. ADC maps were generated after the noise correction, and ADC values of the first five diffusivity levels were recorded.

2.C. In vivo study

The in vivo study was approved by our institutional review board and each subject provided written informed consent. Eight patients were recruited, including two glioblastoma (GBM) patients and six sarcoma patients. Imaging was acquired immediately after the patient's treatment (on ViewRay or other treatment systems). The DW-ssEPI sequence parameters included: FOV = 350−400 × 350−400 mm^2, matrix size = 128 × 128, b = 0, 200, and 500 s/mm^2, 6 mm slices, five averages, and total acquisition time = 32 s. The DP-TSE were acquired at ~3 times finer resolution with the following sequence parameters: FOV = 350−400 × 350−400 mm^2, matrix size = 192 × 192, b = 0, 200, and 500 s/mm^2, 5 mm slices, two averages, and total acquisition time = 108 s. Diffusion gradients were only applied along the readout direction at the current sequence verification stage. A total of 12-channel surface coils were used in the sarcoma patients, and 10-channel head-and-neck coils were used in the GBM patients.

Quantitative geometric accuracy assessment was evaluated using target registration error (TRE)[24]. The reference images, namely patient simulation CT images for the two GBM patients and imaging-day clinical balanced steady-state free precession (bSSFP) MR images for the six sarcoma patients, were rigidly registered to the diffusion imaging plane prior to the analysis. Seven to 12 landmarks were selected for each patient on the reference images, the DW-ssEPI images, and the DP-TSE images, respectively, by a radiation oncologist. These landmarks were easily identifiable structures such as eyeball, CSF, skull, and tumor in GBM patients; muscle group, bone marrow, and tumor in sarcoma patients. Four corners of large size structures were identified to evaluate shape distortions. TRE was calculated as the Euclidean

distance difference between the locations of landmarks on the diffusion images and on the reference images.

ADC accuracy was compared between DW-ssEPI and DP-TSE. In the two GBM patients, ROIs were drawn inside the surgical cavity, the CSF, and the white matter in the DW-ssEPI and DP-TSE images, respectively. For the six sarcoma patients, ROIs were drawn inside the tumor region. ADCs estimated from the two techniques were compared. For patients not treated, only imaged, on ViewRay, a tube phantom containing diluted gadolinium contrast and agarose gel was placed next to the patient when they were brought to ViewRay for imaging. The phantom was not placed on patients treated on ViewRay to avoid interference with treatments. The phantom served as a quality control to monitor the stability of the longitudinal diffusivity measurements in a different study, and is used in this study to show the agreement in ADC measurement between the two sequences.

3. RESULTS

3.A. Quantitative phantom experiment

3.A.1. Spatial integrity

DP-TSE passed the spatial integrity test of < 1 mm discrepancy within 100 mm radius and < 2 mm discrepancy within 175 mm radius in all three orientations while DW-ssEPI did not. The errors between the detected cylinder center locations based on DP-TSE and the known ground truth locations were: 0.474 mm ± 0.355 mm in the axial plane, 0.475 mm ± 0.287 mm in the coronal plane, and 0.546 mm ± 0.336 mm in the sagittal plane. The maximum errors in the three orientations were 1.993 mm, 1.281 mm, and 1.388 mm, respectively. As shown in Fig. 3, due to severe distortion and low signal intensity of the DW-ssEPI images, the software failed to detect the cylinder markers in any of the three orientations using DW-ssEPI images.

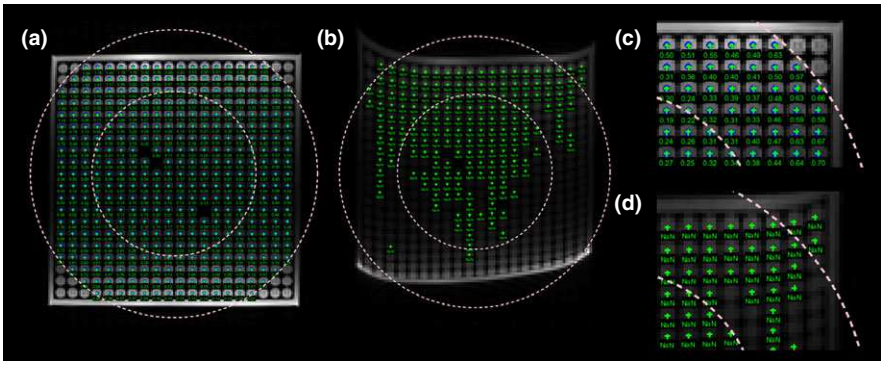

FIG. 3. Phantom images (transverse view) acquired at iso-center using the proposed DP-TSE (a) and the DW-ssEPI (b) techniques with b = 0. (c) and (d) are corresponding zoomed-in images. The green crosses represent the detected marker locations based on the image, and the blue circles are the ground truth marker locations. The DW-ssEPI image has substantial distortions. The detected location was compared with the ground truth for accuracy. A "NaN" would return if the software failed to detect the three missing markers for localization. [Color figure can be viewed at wileyonlinelibrary.com]

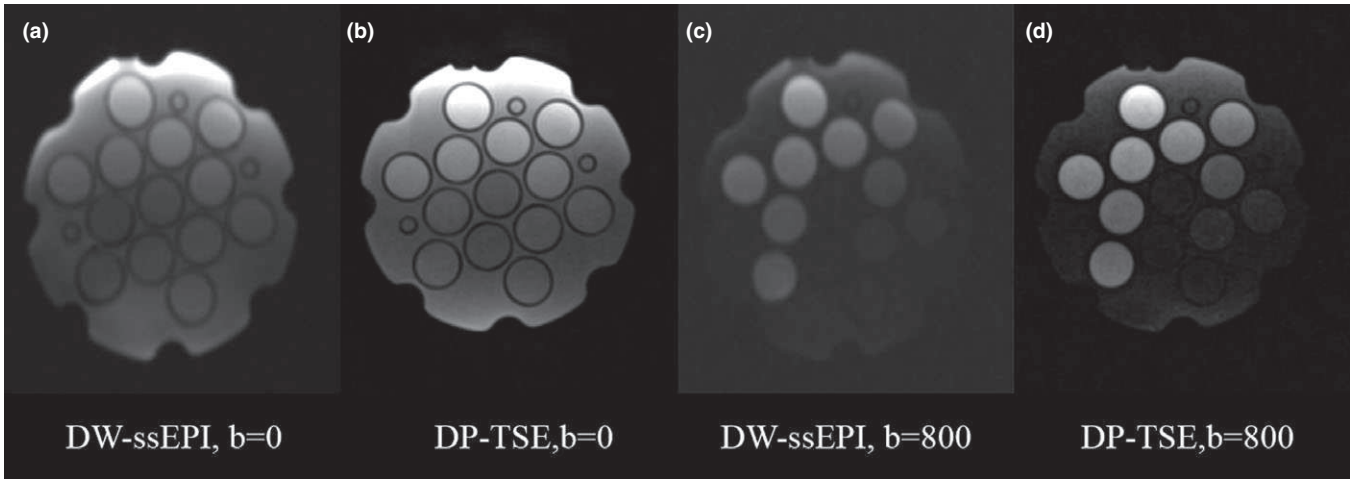

FIG. 4. Raw images of DW-ssEPI (MeR) and DP-TSE (HiR) at b = 0 and b = 800.

3.A.2. ADC accuracy

Figure 4(a)–4(d) are b = 0 and b = 800 images of DW-ssEPI and DP-TSE under room temperature study. Same window level was used for b = 0 and b = 800, respectively. The average background signal intensity of DW-ssEPI was about four times higher than that of DP-TSE, and the signal from the central pure water vial approached to the noise floor level at b = 800. Compared with DW-ssEPI, the proposed DP-TSE had higher resolution, lower background noise level, and less distortion.

Figure 5 demonstrated the effect of noise correction on the central water vial at 0 °C and 21 °C. Because the signal of the EPI approached the noise floor at a modest b-value of 500–800, which usually does not happen at higher field strengths, the data points before noise subtraction [blue line with circle markers in (a) and (c)] deviated from a straight line in the logarithm scale when the b-value gets into the

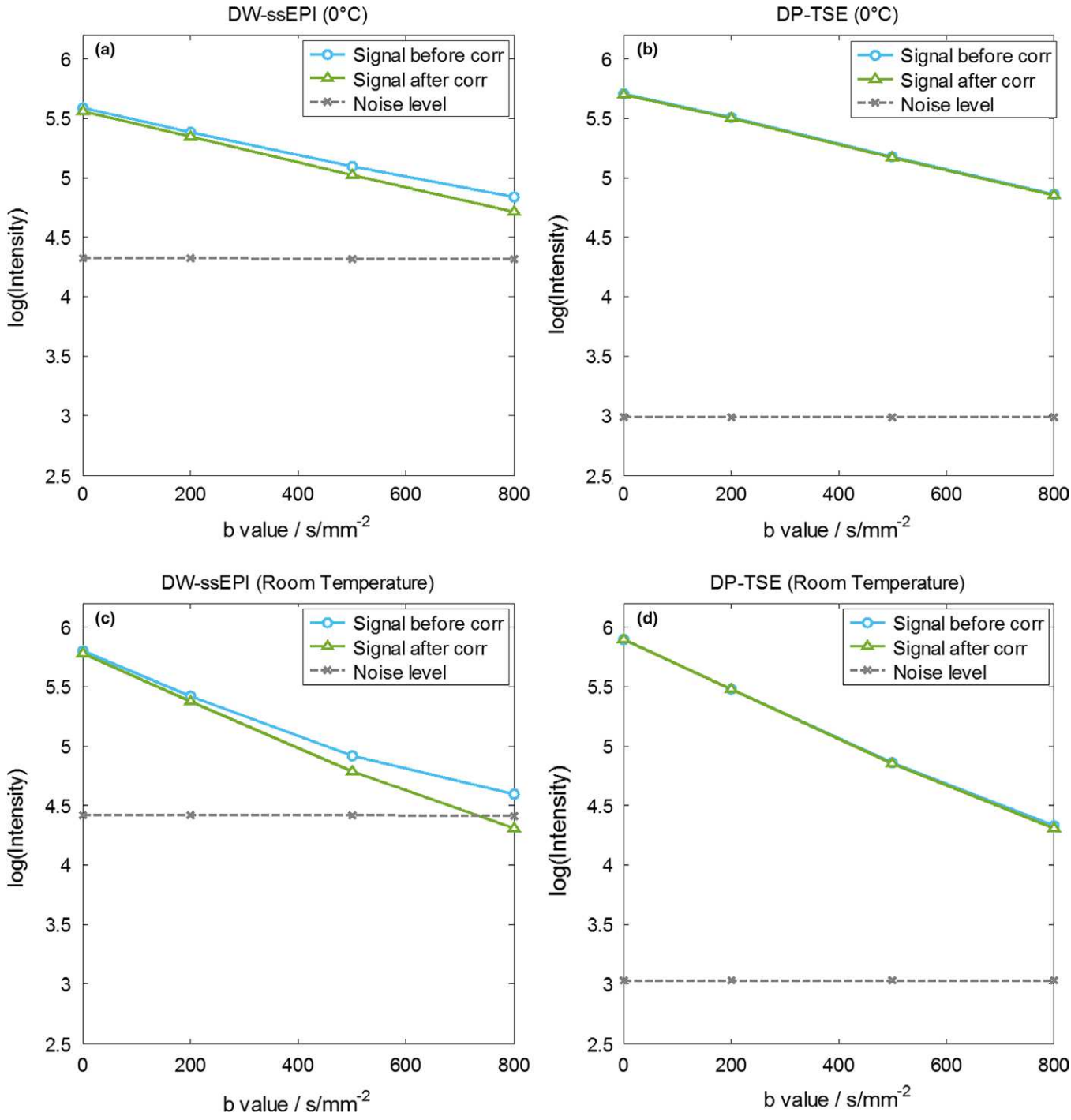

FIG. 5. Effect of noise subtraction on ADC calculation based on DW-ssEPI (a, c) and DP-TSE (b, d) techniques at 0 °C (a, b) and room temperature (c, d). [Color figure can be viewed at wileyonlinelibrary.com]

range of 500–800 s/mm^2. This subsequently resulted in substantial underestimation of the ADC if the mono-exponential fit is used without noise correction. Following noise subtraction [green line with triangle markers in (a) and (c)], the data points displayed improved linearity. For the TSE case in plot (b) and (d), the data before and after noise reduction were both fairly linear, mainly because the TSE signal did not approach the noise floor until much higher b-values of $>$ 1400 s/mm^2.

Figure 6 shows the ADC before and after noise correction at 0 °C and room temperature (21.0 °C in the ViewRay study and 21.8 °C in the 3 T study). Noise subtraction must be performed in DW-ssEPI, otherwise there will be a 12% underestimation and 25% underestimation for vial 1 at 0 °C and room temperature, respectively, using our fit model without noise correction. ADC elevations through noise correction were within 1.5% for DP-TSE, therefore the noise correction step is optional for DP-TSE.

ADC accuracy results after noise subtraction are summarized in Table 1. Under 0 °C, the difference between measured ADCs and reference ADCs were within 3% for both sequences. For the room temperature study, DP-TSE had higher accuracy than DW-ssEPI: discrepancies between ADCs from DP-TSE and the reference were within 4%, but were as high as 8% (vial 1) for DW-ssEPI. However, ADCs from DP-TSE had a higher standard deviation than DW-ssEPI, probably due to lower number of averages used.

3.A.3. ADC reproducibility

In the reproducibility study, the pre-scan temperature of the phantom was 20.68 ± 0.28 °C, and temperature changes after the scans were all within 0.2 °C. Mean ADCs across the ten measurements were: 2.10 ± 0.04 × 10^{-3} mm^2/s for vial 1; 1.62 ± 0.03 × 10^{-3} mm^2/s for vial 2; 1.19 ± 0.02 × 10^{-3} mm^2/s for vial 3; 0.88 ± 0.03 × 10^{-3} mm^2/s for vial 4; and 0.61 ± 0.03 × 10^{-3} mm^2/s for vial 5. The maximum coefficient of variation was below 5% indicating acceptable reproducibility of the proposed technique.

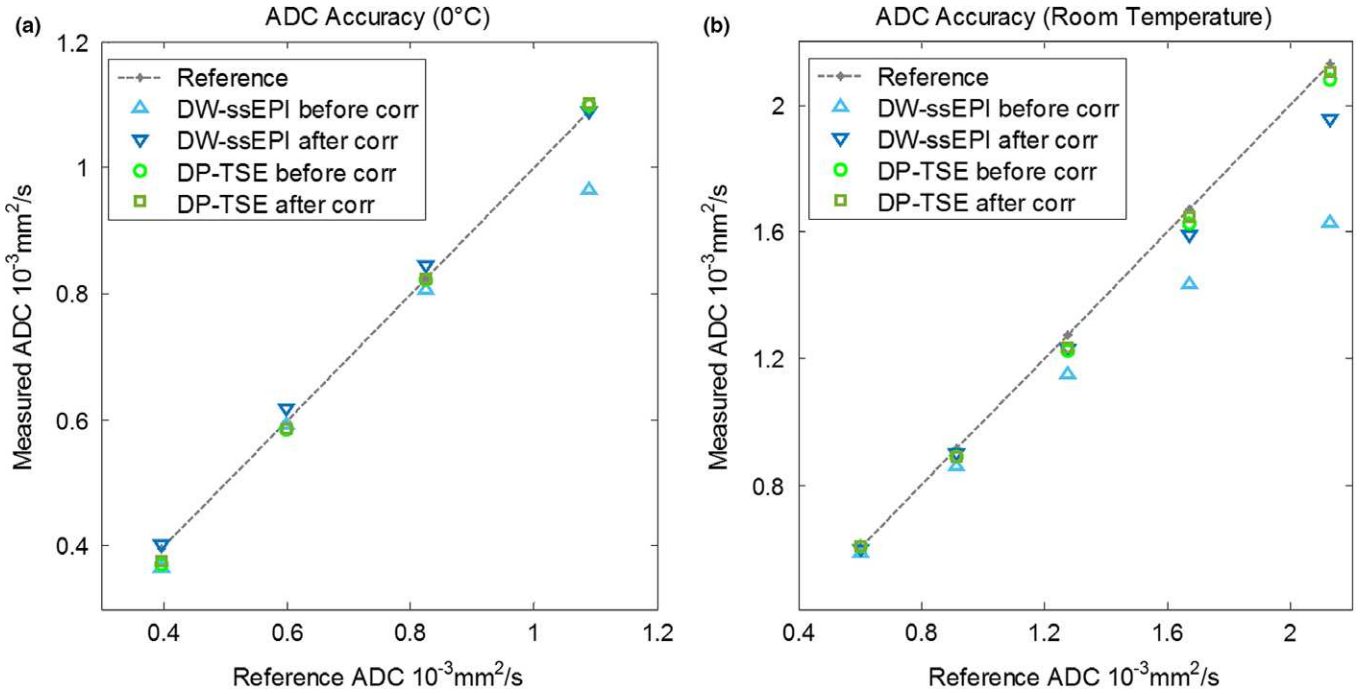

FIG. 6. ADC Accuracy after noise subtraction for DW-ssEPI (MeR) and DP-TSE (HiR) at 0 °C (a) and room temperature (b). [Color figure can be viewed at wileyonlinelibrary.com]

TABLE 1. ADC accuracy results at 0 °C and room temperature.

	0 °C				Room temperature			
	Ref	EPI Mr	Dp-TSE MeR	DP-TSE HiR	Ref	EPI Mr	Dp-TSE MeR	DP-TSE HiR
Vial1	1.09	1.09±0.02	1.11±0.03	1.10±0.06	2.13	1.96±0.04	2.13±0.08	2.10±0.09
Vial2	0.82	0.85±0.02	0.83±0.02	0.82±0.04	1.67	1.59±0.03	1.64±0.05	1.63±0.07
Vial3	0.60	0.62±0.02	0.59±0.02	0.59±0.04	1.27	1.23±0.02	1.22±0.04	1.20±0.06
Vial4	0.40	0.40±0.03	0.39±0.03	0.38±0.04	0.91	0.90±0.03	0.89±0.03	0.89±0.05
Vial5					0.60	0.60±0.04	0.61±0.05	0.61±0.05

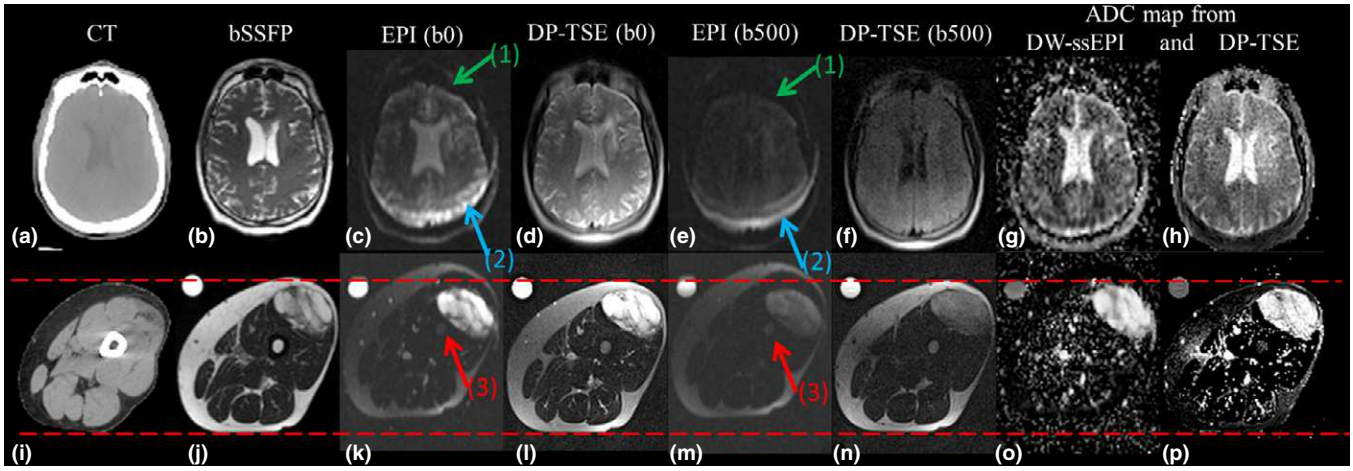

FIG. 7. A comparison from two representative patients. (a)–(h) are the CT, clinical MR image from the standard ViewRay bSSFP sequence, DW-ssEPI (b = 0), DP-TSE(b = 0), DW-ssEPI (b = 500), DP-TSE(b = 500), and ADC maps calculated from DW-ssEPI and DP-TSE on one GBM patient, respectively. (i)–(p) are corresponding images for a sarcoma patient. The green arrows (1) and blue arrows (2) point to signal pile-up and distortion artifacts in the DW-ssEPI image. The red arrows (3) and red dotted lines indicate chemical shift artifacts of the bone marrow and subcutaneous fat. For each patient, the four diffusion-weighted raw images were displayed at the same window level. [Color figure can be viewed at wileyonlinelibrary.com]

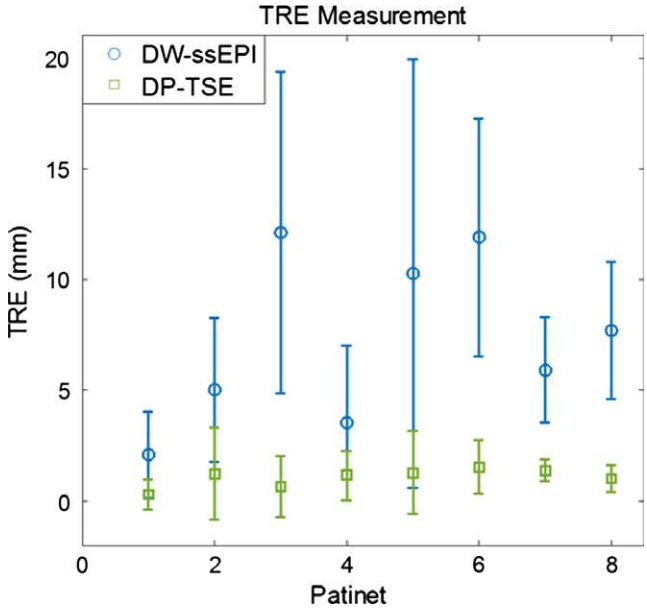

FIG. 8. TRE measurements based on DW-ssEPI and DP-TSE. [Color figure can be viewed at wileyonlinelibrary.com]

TABLE 2. In vivo ADC measurement results.

ADC Measurement ($\times 10^{-3}$ mm^2/s)	DW-ssEPI	DP-TSE
PT1, GBM		
Tumor	2.02±0.48	2.29±0.65
CSF	2.90±0.50	3.17±0.66
White matter	0.56±0.13	0.75±0.33
PT2, GBM		
Tumor	1.04±0.24	1.22±0.33
CSF	2.88±0.43	3.03±0.48
White matter	0.62±0.22	0.76±0.13
PT3-8, Sarcoma		
Tumor	2.60±0.17	2.82±0.45
Tumor	2.34±0.34	2.53±0.72
Tumor	2.67±0.21	2.75±0.37
Tumor	1.28±0.45	1.29±0.60
Tumor	2.70±0.32	2.76±0.44
Tumor	0.65±0.21	0.68±0.28
Vial	1.13±0.04	1.18±0.06

3.B. In vivo study

Figure 7 shows a comparison between DW-ssEPI and DP-TSE from two representative patients. Geometric distortion (green arrows (1)), chemical shift artifacts of the bone marrow and subcutaneous fat (red arrows (3) and dotted lines), and susceptibility related signal pile up (blue arrows (2)) were apparent in the DW-ssEPI images. DP-TSE provided considerably improved geometric accuracy and eliminated chemical shift from fat.

Quantitative landmark TRE measurement results are shown in Fig. 8. The mean TRE was within 1.6 mm for DP-TSE across all eight patients, whereas this value was as high as 12 mm for DW-ssEPI. DW-ssEPI also had a high TRE standard deviation due to the fact that distortion is more apparent along the phase encoding direction and less severe in the readout direction so that the measurements had variations depending on the landmark locations.

Table 2 is a summary of the ADC measurements on all eight patients. In the two GBM patients, ADC values estimated from DP-TSE sequence for CSF and white matter were within literature ranges, which are 2.40×10^{-3}–4.40×10^{-3} mm^2/s for CSF, and 0.60×10^{-3}–1.05×10^{-3} mm^2/s for white matter[25]. White matter ADCs from DW-ssEPI were around the lower limit of the literature value because the low T2 value of white matter aggravated the signal loss, which translated to ADC quantitation

inaccuracy. The tumor ADCs from DW-ssEPI were about 12% and 15% higher than that from DW-ssEPI. Among the six sarcoma patients, the ADCs difference was within 8%. For the reference tube that had a relatively low diffusivity, the two techniques provided matched measurements.

4. DISCUSSION

To the best of our knowledge, the current work is the first in vivo study of a distortion-free diffusion imaging technique using a low-field MRI-guided radiotherapy system. Our results show that the proposed DP-TSE technique provides good ADC quantitation accuracy and substantially improved geometric fidelity when compared with the conventional single-shot EPI approach.

Distortion associated with phase accumulations during the EPI readout is a major problem for applying conventional EPI-based diffusion techniques to MR-guided radiotherapy workflow, even at a low field strength of 0.35 T. TSE, on the other hand, is insensitive to B_0 and off-resonance related artifacts due to the use of 180° refocusing pulses. As shown by the spatial integrity test, our proposed technique provided excellent geometric accuracy with a mean distortion of less than 0.6 mm. The improved geometric fidelity is crucial for future adaptive radiotherapy techniques based on longitudinal onboard ADC measurements[12].

Diffusion imaging requires sufficient SNR in the k-space data to avoid ADC quantitation errors, which occurs when the signal approaches the noise floor level after diffusion attenuation[23]. The problem is further aggravated when the diffusion data are acquired using a low field system like ours, which lowers the magnetic field strength to reduce electron returning effect[26]. In addition, our system has a maximum gradient amplitude of 18 mT/m, and hence requires a long TE for moderate b-values, which consequently reduces SNR. Although TE can be reduced using a higher readout bandwidth, our preliminary results showed that this led to an even lower SNR and inaccurate ADC quantitation. As a consequence, the DW-ssEPI technique required a noise subtraction step before quantitating the ADC. For a low field strength of 0.35 T, the low SNR using the EPI approach might limit the maximum achievable b-value. Our DP-TSE approach was able to achieve a shorter TE (115 ms for DP-TSE vs. 160 ms DW-ssEPI) due to the use of a diffusion preparation module, and it uses a segmented k-space sampling strategy to further boost the signal level compared to the single-shot EPI approach. Therefore, our DP-TSE signal does not approach the noise floor for a typical range of b-values of 100–1000 s/mm^2 and a noise subtraction step is not strictly needed when using our DP-TSE approach. Besides the noise subtraction method implemented in this paper, there are several other methods that handle the noise in diffusion data, such as including the noise in the fitting[27].

Concomitant fields are generally of concern at low field strengths, and they could lead to errors in our ADC quantitation[28,29]. In this study, our sequences have a standard vendor provided concomitant field correction module and the imaging slice was prescribed at the iso-center, which should reduce the concomitant field effects. However, we did not assess the effects of any remaining concomitant field on our ADC accuracy.

It is well known that k-space segmented diffusion acquisitions are vulnerable to signal inconsistencies between different k-space segments because these segments are acquired at different time points and are subject to different signal phase accrual due to motion and system imperfections. Several studies have been proposed to deal with motion-related artifacts in segmented TSE-based diffusion MRI. Pipe et al. implemented a diffusion-weighted PROPELLER TSE sequence, where phase cycling was used to mitigate the magnitude oscillation caused by the non-CPMG components[30]. The PROPELLER trajectory is robust to bulk motion and is self-navigated for phase correction, however, at the expense of about 50% increase of acquisition time compared with Cartesian sampling[30]. In a separate study, a self-navigated interleaved spiral diffusion MRI method with TSE readouts was proposed[31]. Although the 3D acquisition enabled higher resolution and SNR, only in-plane phase inconsistency was corrected and the CPMG condition was violated in its spiral TSE readouts. A more recent multi-shot Cartesian TSE diffusion study by Zhang et al.[32] used a preparation method proposed by Alsop[33] where an additional 90° pulse and dephasing gradients were used to eliminate the non-CPMG component at the expense of losing half of the signal, and multiplexed sensitivity encoding (MUSE)-based reconstruction[34] was used to estimate and correct the k-space phase inconsistencies. One disadvantage of the MUSE-based method it that the number of k-space segments is limited because each segment needs to have a sufficient number of k-space lines for accurately estimating the phase variation maps.

In this study, we chose the traditional Cartesian k-space sampling due to its widespread utility in clinical and research studies. A major difference between our TSE technique and most previously described techniques[30–32] is that we used a stand-alone diffusion preparation module before the imaging readout while most previous techniques used a diffusion-weighted strategy whereby diffusion encoding is a part of the imaging readout. The diffusion preparation strategy eliminates any violation of the CPMG condition in the TSE readout. In our TSE diffusion implementation, we changed the k-space view ordering to ensure that the central k-space lines were acquired in a single shot, which appears to have mitigated any ghosting artifacts in our patient cohort.

Our DP-TSE technique has limitations. Similar to other segmented diffusion MRI techniques, the proposed DP-TSE technique requires a longer scan time when compared with conventional single-shot EPI diffusion techniques. The trade-off between scan time and improved SNR and/or geometric accuracy needs to be balanced for different applications. The current work mainly focuses on phantom verification and in vivo feasibility demonstration. Larger patient cohort studies are warranted to demonstrate the value of this technique in clinical radiotherapy workflow.

5. CONCLUSION

A diffusion-prepared TSE-based diffusion technique with excellent geometric fidelity, accurate and highly reproducible ADC measurement was proposed and verified for longitudinal tumor response assessment using an MRI-guided radiotherapy system.

ACKNOWLEDGMENTS

The authors thank the referees for their valuable and insightful comments during the peer review process.

The authors acknowledge research support from ViewRay, Inc.

CONFLICT OF INTEREST

The authors have no conflict of interest to disclose.

[a)]Author to whom correspondence should be addressed. Electronic mail: penghu@mednet.ucla.edu.

REFERENCES

1. Padhani AR, Liu G, Mu-Koh D, et al. Diffusion-weighted magnetic resonance imaging as a cancer biomarker: consensus and recommendations. *Neoplasia*. 2009;11:102–125.
2. Tsien C, Cao Y, Chenevert T. Clinical applications for diffusion magnetic resonance imaging in radiotherapy. *Semin Radiat Oncol*. 2014; 24:218–226.
3. Tomura N, Narita K, Izumi J, et al. Diffusion changes in a tumor and peritumoral tissue after stereotactic irradiation for brain tumors: possible prediction of treatment response. *J Comput Assist Tomogr*. 2006;30: 496–500.
4. Malayeri AA, El Khouli RH, Zaheer A, et al. Principles and applications of diffusion-weighted imaging in cancer detection, staging, and treatment follow-up. *Radiogr Rev Publ Radiol Soc N Am Inc*. 2011;31:1773–1791.
5. Thoeny HC, Ross BD. Predicting and monitoring cancer treatment response with DW-MRI. *J Magn Reson Imaging JMRI*. 2010;32:2–16.
6. Sharma U, Danishad KKA, Seenu V, Jagannathan NR. Longitudinal study of the assessment by MRI and diffusion-weighted imaging of tumor response in patients with locally advanced breast cancer undergoing neoadjuvant chemotherapy. *NMR Biomed*. 2009;22:104–113.
7. Li SP, Padhani AR. Tumor response assessments with diffusion and perfusion MRI. *J Magn Reson Imaging JMRI*. 2012;35:745–763.
8. Kuang F, Yan Z, Wang J, Rao Z. The value of diffusion-weighted MRI to evaluate the response to radiochemotherapy for cervical cancer. *Magn Reson Imaging*. 2014;32:342–349.
9. Choi SP, Park KN, Park HK, et al. Diffusion-weighted magnetic resonance imaging for predicting the clinical outcome of comatose survivors after cardiac arrest: a cohort study. *Crit Care Lond Engl*. 2010;14:R17.
10. King AD, Chow K-K, Yu K-H, et al. Head and neck squamous cell carcinoma: diagnostic performance of diffusion-weighted MR imaging for the prediction of treatment response. *Radiology*. 2013;266:531–538.
11. Liu L, Wu N, Ouyang H, Dai J-R, Wang W-H. Diffusion-weighted MRI in early assessment of tumour response to radiotherapy in high-risk prostate cancer. *Br J Radiol*. 2014;87:20140359.
12. Yang Y, Cao M, Sheng K, et al. Longitudinal diffusion MRI for treatment response assessment: preliminary experience using an MRI-guided tri-cobalt 60 radiotherapy system. *Med Phys*. 2016;43:1369–1373.
13. Zaharchuk G, Saritas EU, Andre JB, et al. Reduced field-of-view diffusion imaging of the human spinal cord: comparison with conventional single-shot echo-planar imaging. *AJNR Am J Neuroradiol*. 2011;32:813–820.
14. Gudbjartsson H, Maier SE, Mulkern RV, Mórocz IÁ, Patz S, Jolesz FA. Line scan diffusion imaging. *Magn Reson Med*. 1996;36:509–519.
15. Chang H, Fitzpatrick JM. A technique for accurate magnetic resonance imaging in the presence of field inhomogeneities. *IEEE Trans Med Imaging*. 1992;11:319–329.
16. Porter DA, Heidemann RM. High resolution diffusion-weighted imaging using readout-segmented echo-planar imaging, parallel imaging and a two-dimensional navigator-based reacquisition. *Magn Reson Med*. 2009; 62:468–475.
17. Jeong E-K, Kim S-E, Parker DL. High-resolution diffusion-weighted 3D MRI, using diffusion-weighted driven-equilibrium (DW-DE) and multishot segmented 3D-SSFP without navigator echoes. *Magn Reson Med*. 2003;50:821–829.
18. Nguyen C, Fan Z, Sharif B, et al. *In vivo* three-dimensional high resolution cardiac diffusion-weighted MRI: a motion compensated diffusion-prepared balanced steady-state free precession approach. *Magn Reson Med*. 2014;72:1257–1267.
19. Xie Y, Yu W, Fan Z, et al. High resolution 3D diffusion cardiovascular magnetic resonance of carotid vessel wall to detect lipid core without contrast media. *J Cardiovasc Magn Reson*. 2014;16:67.
20. Reese TG, Heid O, Weisskoff RM, Wedeen VJ. Reduction of eddy-current-induced distortion in diffusion MRI using a twice-refocused spin echo. *Magn Reson Med*. 2003;49:177–182.
21. Robson MD, Anderson AW, Gore JC. Diffusion-weighted multiple shot echo planar imaging of humans without navigation. *Magn Reson Med*. 1997;38:82–88.
22. Bammer R, Holdsworth SJ, Veldhuis WB, Skare ST. New methods in diffusion weighted and diffusion tensor imaging. *Magn Reson Imaging Clin N Am*. 2009;17:175–204.
23. Dietrich O, Heiland S, Sartor K. Noise correction for the exact determination of apparent diffusion coefficients at low SNR. *Magn Reson Med*. 2001;45:448–453.
24. Maurer CR, Fitzpatrick JM, Wang MY, Galloway RL, Maciunas RJ, Allen GS. Registration of head volume images using implantable fiducial markers. *IEEE Trans Med Imaging*. 1997;16:447–462.
25. Sener RN. Diffusion MRI: apparent diffusion coefficient (ADC) values in the normal brain and a classification of brain disorders based on ADC values. *Comput Med Imaging Graph*. 2001;25:299–326.
26. Raaijmakers AJE, Raaymakers BW, Lagendijk JJW. Magnetic-field-induced dose effects in MR-guided radiotherapy systems: dependence on the magnetic field strength. *Phys Med Biol*. 2008;53:909.
27. Iima M, Yano K, Kataoka M, et al. Quantitative non-Gaussian diffusion and intravoxel incoherent motion magnetic resonance imaging: differentiation of malignant and benign breast lesions. *Invest Radiol*. 2015;50:205–211.
28. Baron CA, Lebel RM, Wilman AH, Beaulieu C. The effect of concomitant gradient fields on diffusion tensor imaging. *Magn Reson Med*. 2012;68:1190–1201.
29. Aliotta E, Wu HH, Ennis DB. Convex optimized diffusion encoding (CODE) gradient waveforms for minimum echo time and bulk motion–compensated diffusion-weighted MRI. *Magn Reson Med*. 2017;77:717–729.
30. Pipe JG, Farthing VG, Forbes KP. Multishot diffusion-weighted FSE using PROPELLER MRI. *Magn Reson Med*. 2002;47:42–52.
31. Frank LR, Jung Y, Inati S, Tyszka JM, Wong EC. High efficiency, low distortion 3D diffusion tensor imaging with variable density spiral fast spin echoes (3D DW VDS RARE). *NeuroImage*. 2010;49:1510–1523.
32. Zhang Z, Zhang B, Li M, et al. Multishot cartesian turbo spin-echo diffusion imaging using iterative POCSMUSE Reconstruction. *J Magn Reson Imaging*. 2017;46:167–174.
33. Alsop DC. Phase insensitive preparation of single-shot RARE: application to diffusion imaging in humans. *Magn Reson Med*. 1997;38:527–533.
34. Chen N-K, Guidon A, Chang H-C, Song AW. A robust multi-shot scan strategy for high-resolution diffusion weighted MRI enabled by multiplexed sensitivity-encoding (MUSE). *NeuroImage*. 2013;72:41–47.

ClearCheck

One-click plan evaluation

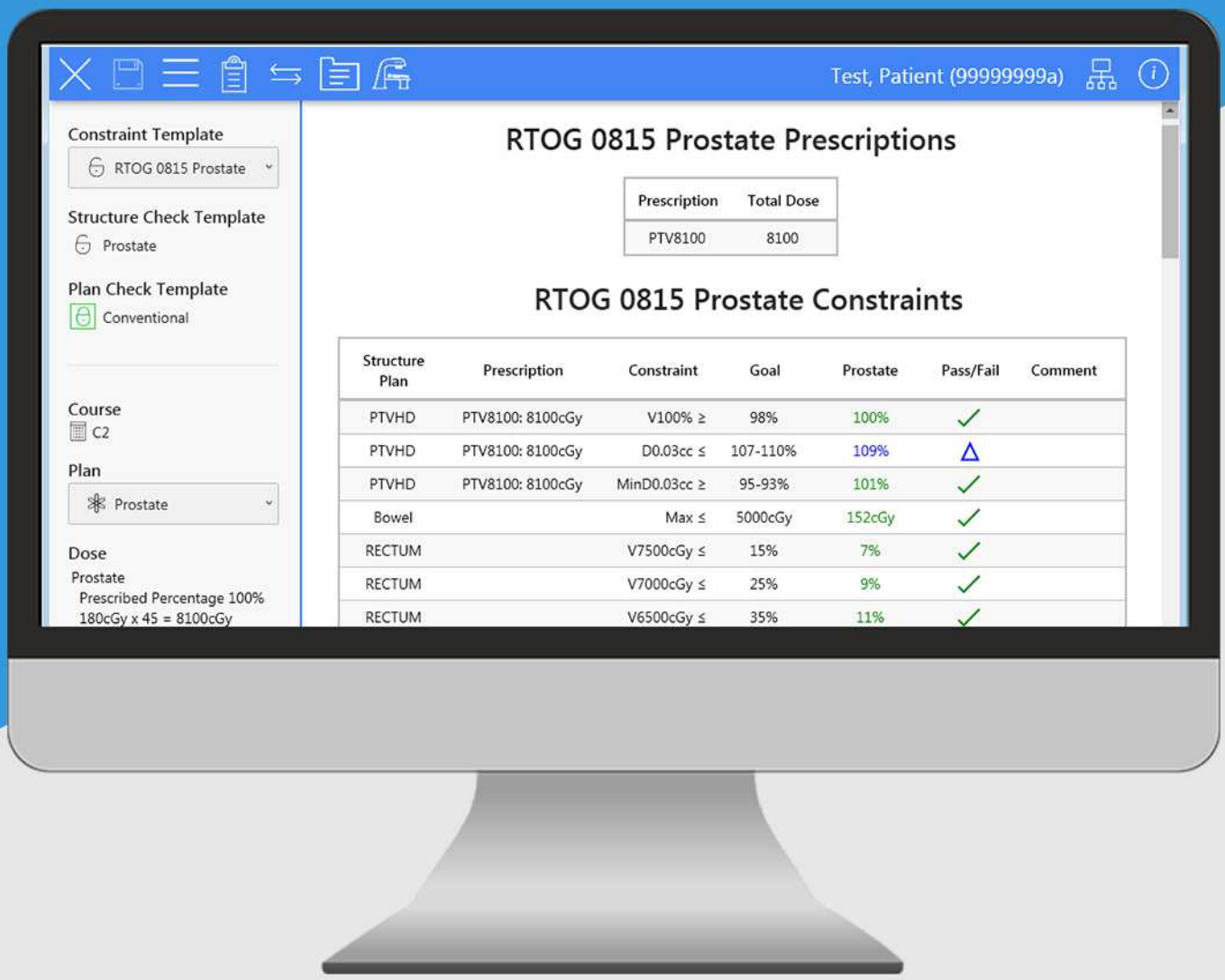

Dose Constraints ◦ Plan Checks

Structure Checks ◦ Collision Checks

RADformation.com